SCIENCE CHINA
Chemistry

•ARTICLES•
SPECIAL ISSUE: 2021 Emerging Investigator Issue

November 2021 Vol.64 No.11: 2017–2024
https://doi.org/10.1007/s11426-021-1114-3

Synergistic effect of solvent and solid additives on morphology optimization for high-performance organic solar cells

Chenling Fan[1], Hang Yang[1], Qing Zhang[3], Sunan Bao[1], Hongyu Fan[1], Xianming Zhu[1], Chaohua Cui[1*] & Yongfang Li[1,2]

[1]*Laboratory of Advanced Optoelectronic Materials, Suzhou Key Laboratory of Novel Semiconductor-Optoelectronics Materials and Devices, College of Chemistry, Chemical Engineering and Materials Science, Soochow University, Suzhou 215123, China;*
[2]*Beijing National Laboratory for Molecular Sciences, CAS Key Laboratory of Organic Solids, Institute of Chemistry, Chinese Academy of Sciences, Beijing 100190, China;*
[3]*Vacuum Interconnected Nanotech Workstation, Suzhou Institute of Nano-Tech and Nano-Bionics, Chinese Academy of Sciences, Suzhou 215123, China*

Received June 14, 2021; accepted September 6, 2021; published online September 15, 2021

Controlling the photoactive layer morphology towards nanoscale bi-continuous donor/acceptor interpenetrating networks is a key issue to build high-performance organic solar cells (OSCs). Due to the distinct properties between donor and acceptor materials, casting an active layer from a single solvent solution usually results in either insufficient or excessive phase separation that reduces the device performance. In comparison to the fullerene acceptors with closed-cage structures, the currently dominant non-fullerene acceptors possess the similar anisotropic π–π interactions with *p*-type organic semiconductor donors, giving rise to the complexity of the morphology regulation. Herein, we employ 4,4′-dimethoxyoctafluorobiphenyl (OFP) with strong crystallinity as a volatile solid additive to optimize the active layer morphology of OSCs. The synergistic effect of 1-chloronaphthalene (CN) and OFP as dual additives shows supreme capability on optimizing the morphology over the conventional additive of CN, which is in favor of improving charge transport and suppressing charge recombination for higher fill factors in various systems. In particular, the PTQ10:*m*-BTP–C6Ph-based device processed by the additive showed a remarkable power-conversion efficiency (PCE) of 17.74%, whereas the control device processed by CN additive yielded a relatively lower PCE of 16.45%.

organic solar cells, bulk-heterojunction morphology, power conversion efficiency, solid additive

Citation: Fan C, Yang H, Zhang Q, Bao S, Fan H, Zhu X, Cui C, Li Y. Synergistic effect of solvent and solid additives on morphology optimization for high-performance organic solar cells. *Sci China Chem*, 2021, 64: 2017–2024, https://doi.org/10.1007/s11426-021-1114-3

1 Introduction

Owing to the attractive features of lightweight, semi-transparency, and flexibility, organic solar cells (OSCs) exhibit great potential applications as a clean-energy photovoltaic technology [1–5]. Photoactive layer which absorbs photons to generate excitons is the key component to determine the photovoltaic performance of the OSCs [6–13]. Bulk-heterojunction (BHJ) layer, in which *p*-type organic semiconductor donors and *n*-type organic semiconductor acceptors are blended together, is the widely used active layer for state-of-the-art OSCs [14,15]. During the past few years, the emerging of non-fullerene acceptors which possess the distinct advantages of broad and tunable absorption features, suitable electronic energy levels, and planar structures significantly pushes forward the development of OSCs [16–21]. To realize high-performance OSCs, well-matching energy levels and complementary absorption spectra be-

*Corresponding author (email: cuichaohua@suda.edu.cn)

tween the donor and acceptor are prerequisite requirements. Additionally, appropriate blend-film morphology of nanoscale phase separation along with bi-continuous interpenetrating network is critical for efficient charge dissociation and transport in a BHJ-OSC [22–24].

The morphology of photovoltaic layers is closely affected by solubility, crystallinity, and miscibility of donor and acceptor materials. Due to the distinct properties between donor and acceptor materials, the BHJ blend film casted from a single solvent solution usually shows either insufficient or excessive phase separation that is unfavorable for device performances. Therefore, morphology control methods are extensively required to tune the phase separation toward enhancing photovoltaic performances for OSCs.

Adding a trace amount of appropriate solvent in host solvent is an effective and widely used strategy to manipulate the morphology of BHJ-OSCs [23–29]. A key point for this method is that the solvent additive should possess selective solubility to donors and acceptors. On this premise, the solvent additive with lower volatile than the host solvent is in favor of manipulating the aggregation of donors and acceptors toward appropriate phase separation during the film-formation process. Except for solvent additives, solid additives with strong crystallization have demonstrated their positive effect on regulating the self-assembly of photovoltaic materials during the past decades with fullerene derivatives as the dominant acceptors [30–34]. In comparison with the fullerene acceptors with closed-cage structures, the similar anisotropic π–π interactions between non-fullerene acceptors and *p*-type organic semiconductor donors gives rise to the complexity of morphology regulation. Meanwhile, the solvent additives applied for the non-fullerene acceptor-based systems empirically follow those originally developed in fullerene-based systems, being unable to meet the unique features of non-fullerene acceptors. Apparently, it is desirable to develop morphology control approaches to further optimize the morphology of non-fullerene acceptors-based blend films for the improvement of photovoltaic performances.

To overcome the limitation of solvent additives in the non-fullerene systems, in this work, we employ 4,4′-dimethoxyoctafluorobiphenyl (namely OFP, Figure 1) as a volatile solid additive to optimize the morphology. OFP shows strong crystallinity and can be completely volatilized under thermal annealing (TA) at 90 °C for 10 min [35,36]. Used as additive in the non-fullerene-based blend film, OFP can restrict the over aggregation of non-fullerene acceptors with high crystallinity during the film formation process, leaving the well-established phase separation with nanoscale bi-continuous donor/acceptor interpenetrating network after OFP volatilization under TA. As a result, an enhanced power-conversion efficiency (PCE) of 16.78% was achieved in the PM6:Y6-based device processed by the dual additives of OFP and 1-chloronaphthalene (CN), which is higher than that of the control device processed by CN additive alone (PCE=15.70%). Encouragingly, the dual additives of OFP and CN show better outcome on optimizing morphology in various non-fullerene-based blend films than the conventional solvent additive, enabling significantly improved photovoltaic performances. Particularly, a remarkable PCE of 17.74% was yielded in the PTQ10:*m*-BTP-C6Ph-based device processed by the dual additives of OFP and CN, while the control device processed by CN additive alone yielded a lower PCE of 16.45% [37].

2 Results and discussion

To examine the volatility of OFP, thermogravimetry analysis (TGA) was performed. As shown in Figure 1a. OFP exhibited a weight loss starting from approximately 90 °C, along with T_d (5% weight loss) at approximately 109 °C at a scan rate of 10 °C min^{-1}. Additionally, complete weight loss was observed when the temperature held at 90 °C for 1 h (Figure 1b), suggesting the volatility of OFP at this temperature. Then, we performed the Fourier transform infrared (FT-IR) measurement to further prove the volatilization of OFP in the blend film. As depicted in Figure 1c, OFP possesses characteristic FT-IR absorption peaks at 720, 1,000, 1,109, and 1,503 cm^{-1} compared to the PM6:Y6 mixture. By TA at 90 °C for 20 min, four characteristic absorption peaks of OFP vanished in the FT-IR absorption spectroscopy of the PM6:Y6:OFP (1:1.2:1, *w*/*w*) blend film, further confirming that the OFP solid additive can be completely volatized from the blend film after the TA.

To investigate the effect of OFP in morphology optimization, OSCs were fabricated by using a conventional device architecture of ITO/PEDOT:PSS/active layer/PDINO/Al, as shown in Figure 1a. Detailed experimental procedures are provided in the Supporting Information. The key photovoltaic parameters of the optimal PM6:Y6-based device with various additives are summarized Table 1, and the corresponding short-circuit current density-voltage (*J*–*V*) curves are shown in Figure 2a. The optimal active layer thickness of the devices under different additives is 96–102 nm (see Supporting Information). The PM6:Y6 (1:1.2, *w*/*w*)-based device without any additive showed a PCE of 14.85%, along with a open-circuit voltage (V_{OC}) of 0.858 V, a short-circuit current density (J_{SC}) of 24.99 mA cm^{-2}, and a fill factor (FF) of 0.691 (Table 1). The PM6:Y6-based device with the optimal additive of 0.5% CN (*v*/*v*) as solvent additive and TA at 90 °C for 10 min demonstrated a higher PCE of 15.70%, which is consistent with the PCE value reported in literature [18]. Then, OFP was applied as the solid additive in the PM6:Y6 blend to further tune the morphology, followed by TA at 90 °C for 10 min to volatize it from the blend film. As shown

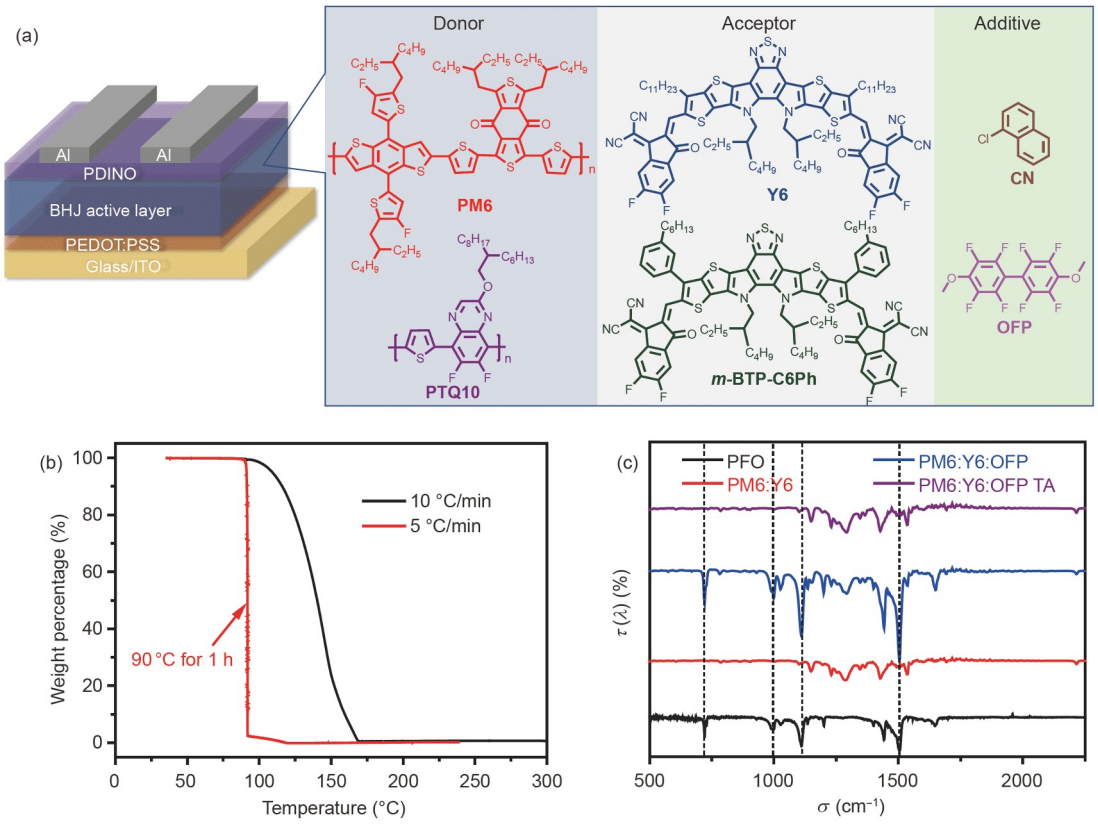

Figure 1 (a) Device structure of the OSC and chemical structures of PM6, Y6, OFP, and CN. (b) TGA plot of OFP at a scan rate of 5 or 10 °C min^{-1} under inert atmosphere. (c) FTIR spectra of OFP, PM6:Y6 (1:1.2 *w*/*w*), PM6:Y6:OFP (1:1.2:1, *w*/*w*), and PM6:Y6:OFP (1:1.2:1, *w*/*w*) after TA at 90 °C for 20 min (color online).

in Table S1 and Figure S1, using 10 or 20% (*w*/*w*, relative to Y6) OFP as the solid additive effectively improved the FF of the PM6:Y6-based device. Encouragingly, the device processed by 20% OFP solid additive showed an improved PCE of 15.43% compared to the control device without any additive (Table 1). Further increasing the OFP concentration to 30% led to slightly lower PCE, due to the overall lower V_{OC}, J_{SC}, and FF.

On account of the positive effect of the OFP solid additive and the CN solvent additive in tuning the morphology of the non-fullerene systems, OFP and CN were simultaneously used as co-additives to further modulate the morphology of PM6:Y6 system. As shown in Table S2 and Figure S2, increasing the concentration of OFP solid additive from 8.3% to 25.0% (relative to Y6, *w*/*w*) simultaneously improved the J_{SC} and FF values of the devices compared to that processed by CN solvent additive, and enabled higher PCEs. Particularly, the dual additive of 25.0% OFP and 0.5% CN led to better photovoltaic performances over the devices processed by only CN solvent additive, showing the higher PCE of 16.76% and the higher FF of 0.770 (Table 1). On the other hand, we noted that the increment of OFP concentration (from 25.0% to 41.7%) in the blend film gradually decreased the V_{oc} (from 0.841 to 0.822 V, respectively, Table S2) of the devices. To understand such phenomena, energy loss analysis in the device was performed, as described in the Supporting Information. The results suggest that the increment of OFP concentration as additive for the PM6:Y6 blend resulted in larger non-radiative recombination loss in the devices (Table S5), which is the major reason of the decreased V_{OC} as observed. Generally, an optimal donor/acceptor interfacial area in the active layer is beneficial to reduce the recombination loss in an OSC [38,39]. Therefore, the reduced non-radiative recombination loss in the device processed by 25.0% OFP compared with the other ratios should be ascribed to the more appropriate phase separation which will be discussed later.

Figure 2b shows the external quantum efficiency (EQE) curves of the PM6:Y6-based devices with different additives. In comparison with the PM6:Y6-based device without any additive, the application of CN solvent additive enhanced the EQE values in the wavelength range of 600–850 nm, and the enhancement is more pronounced by using the dual additives of CN and OFP, corresponding to the higher J_{SC} values. Such enhancement in EQE values is mainly due to the higher absorption coefficient of the blend film with the dual additives (Figure S3). The J_{SC} values integrated from the EQE curves are consistent with that obtained from *J*–*V* measure-

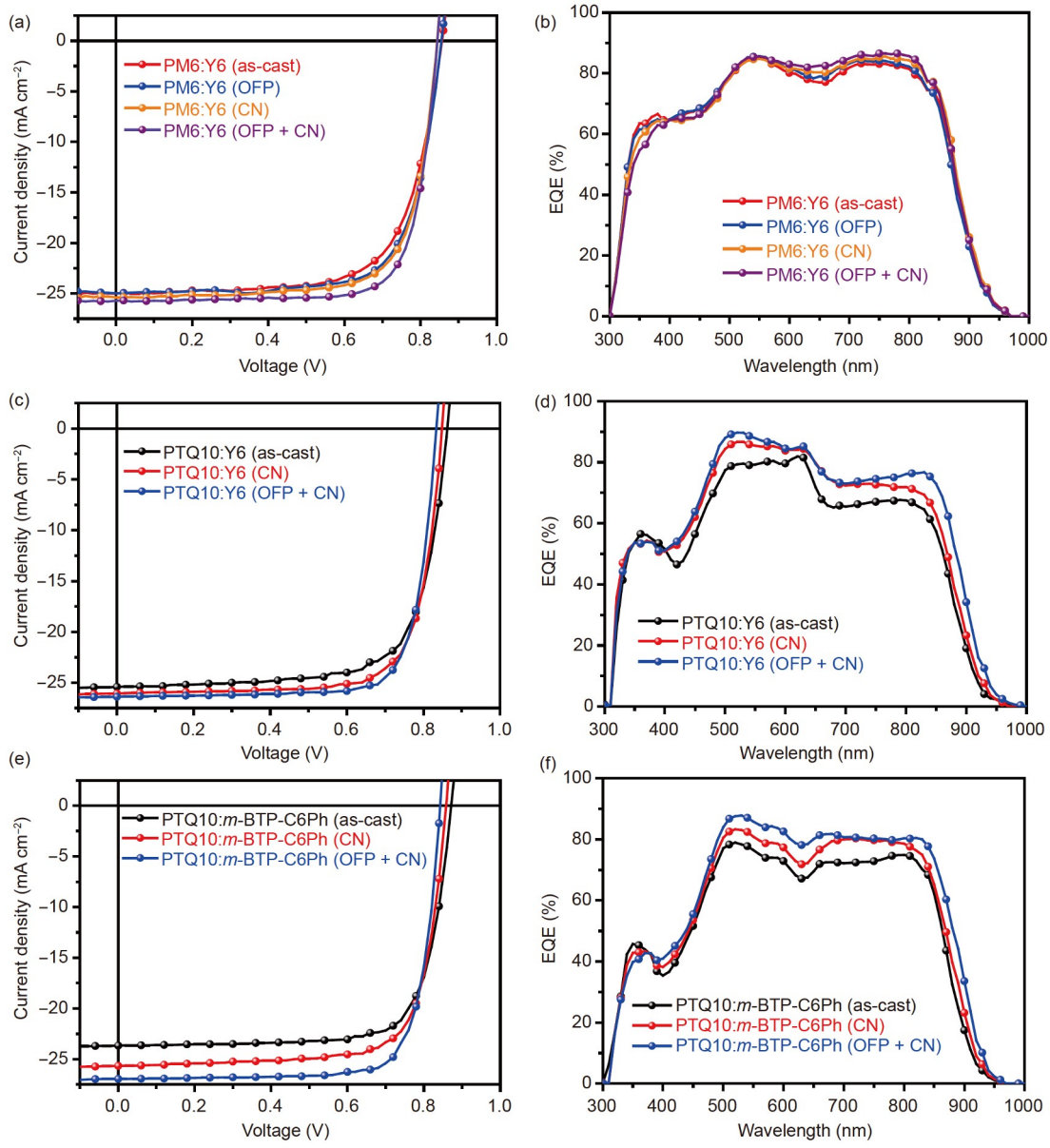

Figure 2 (a) *J*–*V* curves of the PM6:Y6-based OSCs with different additives, under the illumination of AM 1.5G at 100 mW cm^{-2}, (b) EQE spectra of the corresponding OSCs. (c) *J*–*V* curves of the PTQ10:Y6 OSCs with different additives under the illumination of AM 1.5G at 100 mW cm^{-2}, (d) EQE spectra of the corresponding OSCs. (e) *J*–*V* curves of the PTQ10:*m*-BTP–C6Ph-based OSCs with different additives under the illumination of AM 1.5G at 100 mW cm^{-2}. (f) EQE spectra of the corresponding OSCs (color online).

ments.

To further evaluate the positive effect of the dual additives of CN and OFP in other systems, we fabricated the PTQ10:Y6 [40] and PTQ10:*m*-BTP–C6Ph-based OSCs. The key photovoltaic parameters of the devices are summarized in Table 1 and the corresponding *J*–*V* curves are shown in Figure 2c and 2e. The PTQ10:Y6-based device without any additive or processed by 0.5% CN (*v*/*v*) as solvent additive showed a PCE of 15.63% and 16.49%, respectively, which is consistent with our previous report [40]. By using dual additives of CN and OFP, the FF of the device was further improved to 0.784, along with a slightly higher J_{SC} of 26.28 mA cm^{-2} and a slightly lower V_{OC} of 0.831 V, delivering a higher PCE of 17.13% (Table 1). In the case of the PTQ10:*m*-BTP–C6Ph-based device, the device without any additive showed a PCE of 15.66%, while the additive of 0.75% CN (*v*/*v*) led to a higher PCE of 16.45% and a FF of 0.749 (Table 1). Furthermore, the dual additives enabled a significantly higher FF of 0.783 and J_{SC} of 26.95 mA cm^{-2}, resulting in a notable PCE of 17.74%.

Figure 2d and 2f display the EQE spectra of the OSCs based on PTQ10:Y6 and PTQ10:*m*-BTP–C6Ph processed by CN or dual additives of CN and OFP. Compared with the devices using CN as solvent additive, the dual additives of

CN and OFP enhanced the incident photon-to-current conversion efficiency in the wavelength range of 650–850 nm, corresponding to the higher J_{SC} value for the PTQ10:Y6 and PTQ10:*m*-BTP–C6Ph-based OSCs, respectively. The generality of the dual additives of CN and OFP was further confirmed by applying them into the PTQ10:IDIC and PBDB–T:ITIC blends for morphology improvement. As shown in Table S7 and Figure S12, the dual additives of CN and OFP effectively improved the photovoltaic performance of the PTQ10:IDIC and PBDB–T:ITIC-based devices as compared with the control devices without any additive, respectively.

The improvement of PCEs aroused by the dual additives of OFP and CN for the PM6:Y6-based devices is mainly due to the improved FFs, which generally results from the improved charge transport and suppressed recombination. First, the charge transport properties of the blend film were measured by the space-charge-limited current (SCLC) method (experimental details are described in the Supporting Information). As shown in Figure 3a and Figure S6, the PM6:Y6 blend without any additive showed a hole mobility (μ_h) of 3.20×10^{-3} cm^2 V^{-1} s^{-1} and an electron mobility (μ_e) of 1.84×

Table 1 Photovoltaic performances of the PM6:Y6-based OSCs with different additivesunder the illumination of AM 1.5G (100 mW cm^{-2})[a)]

Active layer	Additive	V_{OC} (V)	J_{SC} (mA cm^{-2})	FF	PCE (%)
PM6:Y6	N/A	0.858 (0.858±0.002)	24.99 (24.82±0.36)	0.691 (0.690±0.006)	14.85 (14.71±0.25)
	OFP	0.851 (0.849±0.003)	25.07 (25.12±0.21)	0.724 (0.719±0.006)	15.43 (15.37±0.11)
	CN	0.843 (0.844±0.002)	25.38 (25.19±0.23)	0.734 (0.734±0.005)	15.70 (15.53±0.16)
	OFP+CN	0.841 (0.841±0.002)	25.91 (25.86±0.18)	0.770 (0.766±0.002)	16.78 (16.64±0.16)
PTQ10:Y6	N/A	0.861 (0.860±0.002)	25.33 (25.36±0.19)	0.719 (0.712±0.008)	15.63 (15.53±0.07)
	CN	0.846 (0.843±0.004)	26.00 (25.98±0.09)	0.750 (0.748±0.004)	16.49 (16.37±0.08)
	OFP+CN	0.831 (0.829±0.002)	26.28 (26.41±0.28)	0.784 (0.777±0.007)	17.13 (17.02±0.13)
PTQ10:*m*-BTP-C6Ph	N/A	0.870 (0.870±0.003)	23.72 (23.66±0.09)	0.759 (0.748±0.010)	15.66 (15.39±0.20)
	CN	0.856 (0.853±0.003)	25.66 (25.53±0.15)	0.749 (0.746±0.006)	16.45 (16.23±0.10)
	OFP+CN	0.841 (0.839±0.002)	26.95 (26.79±0.24)	0.783 (0.782±0.007)	17.74 (17.57±0.12)

a) The statistical values in brackets were calculated from 15 devices.

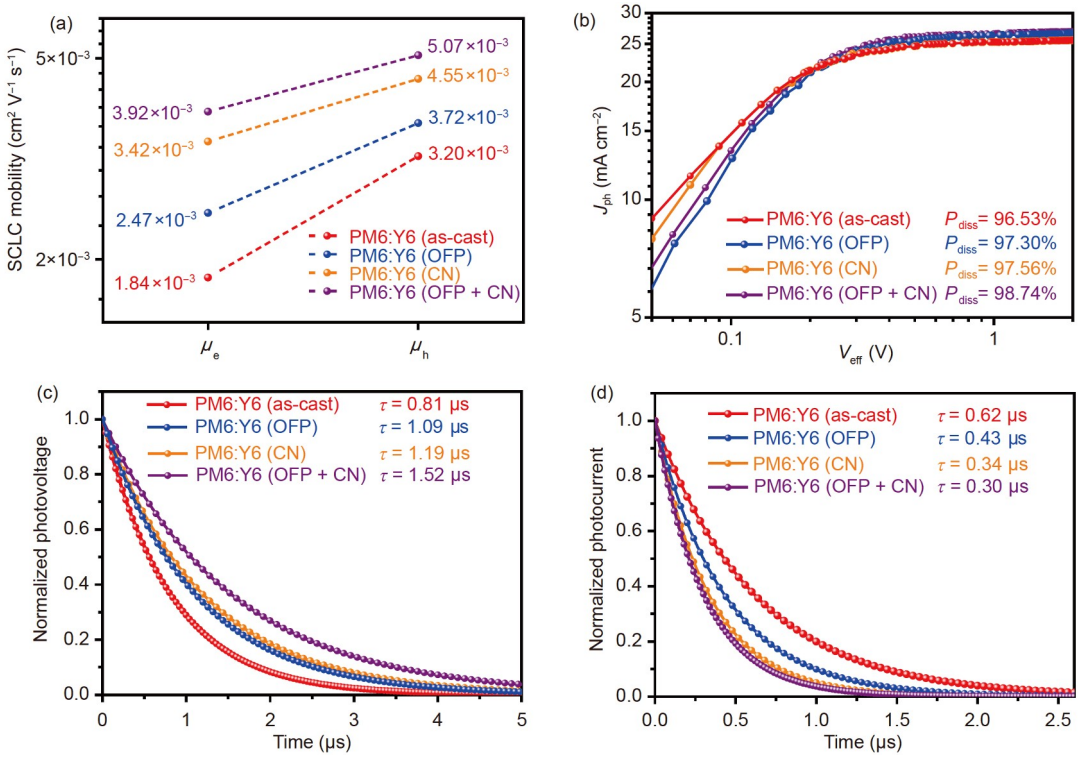

Figure 3 (a) Hole and electron mobilities, (b) the logarithmic curves of J_{ph} *versus* V_{eff}, (c) TPV measurements and (d) TPC measurements of the PM6:Y6-based OSCs with different additives (color online).

10^{-3} cm^2 V^{-1} s^{-1}. Comparatively, using CN or OFP as additives for the blend film enhanced the μ_h and μ_e, and resulted in the higher FF than that of the device without any additive. Especially, the dual additives of CN and OFP effectively enhanced the μ_h and μ_e to 5.07×10^{-3} and 3.92×10^{-3} cm^2 V^{-1} s^{-1}, respectively, which was the highest value compared with the device without/with only CN or OFP additive. Then we plotted the curves of photocurrent density (J_{ph}) (J_{ph}=J_L–J_D, where J_L and J_D represent the light and dark current density, respectively) *versus* the effective voltage (V_{eff}) of the devices to investigate the effect of the additives on the exciton dissociation probability (P_{diss}) [41]. As shown in Figure 3b, relative to the P_{diss} of 96.53% fitted for the PM6:Y6-based device without any additive, the additive of CN or OFP enhanced the P_{diss} to 97.56% and 97.30%, respectively. Moreover, a higher P_{diss} of 98.74% was obtained in the device processed by the dual additives of CN and OFP.

We then plotted the dependence of J_{SC} and V_{OC} on the light intensity (P_{light}) to investigate the charge recombination in the devices with various additives. As depicted in Figure S9, the devices with various additives showed a similar exponential factor (α) which approached 1 (over 0.98), indicating that bimolecular recombination is negligible in the devices [42]. On the other hand, the dual additives for the PM6:Y6-based device effectively reduced the slope (n) (more closer to kT/q (where q is the elementary charge, k is the Boltzmann constant, and T is the Kelvin temperature)) of the curve of $V_{OC}\propto\ln P_{light}$ as compared with the other additives (Figure S9), implying that the trap-assisted charge recombination was suppressed in the devices [43]. Transient photovoltage (TPV) and transient photocurrent (TPC) measurements were performed to evaluate the effect of additives on the carrier lifetime and charge extraction time of the PM6:Y6-based devices. As shown in Figure 3c, the carrier lifetime of the device processed with CN or OFP additive was determined to be 1.09 and 1.19 μs, respectively, which is longer than that of the control device (0.81 μs) without any additive, while the carrier lifetime for the device with the dual additives of CN and OFP was further prolonged to 1.52 μs. Furthermore, the dual additives favor to shorten the charge extraction time compared with the CN or OFP additive, which was determined by the TPC measurement (Figure 3d). Generally, longer carrier lifetime associated with shorter charge extraction time indicates lower recombination rates in the OSCs.

We performed grazing-incidence wide-angle X-ray scattering (GIWAXS) measurements to clarify the effects of the additives on the molecular packing morphology of the blend films. As shown in Figure S10, the neat PM6 and Y6 film exhibited clear π–π stacking (010) peaks at q_z=1.703 (d-spacing=3.68 Å) and 1.755 Å^{-1} (d-spacing=3.58 Å) in the out-of-plane (OOP) direction, with the calculated coherence length (L_c) of 24.6 and 27.0 Å, respectively, indicating the preferable face-on orientation of the molecular packing with respect to the substrate. Relative to the PM6:Y6 blend without any additive, the OFP or CN additive effectively enhanced the π–π stacking (010) peak associated with a higher L_c of 28.5 and 33.5 Å in the OOP direction, and the effect of CN additive was more pronounced (Figure 4). Compared with the only OFP or CN additive, the stronger π–π stacking (010) peak and higher L_c of 38.3 Å were observed in the PM6:Y6 blend processed with the dual additives of OFP and CN, indicating the ordered crystalline structure of the blend film in the vertical direction. It can be concluded

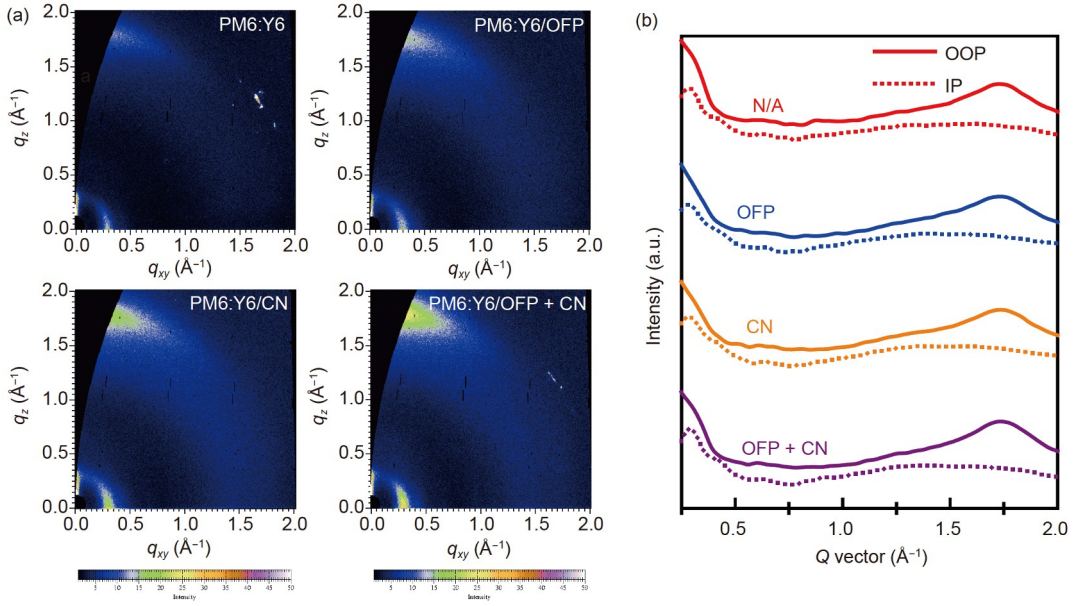

Figure 4 (a) 2D GIWAXS patterns and (b) line-cuts of the PM6:Y6 (1:1.2, *w*/*w*) blend films processed with different additives (color online).

that the synergistic effect of the OFP and CN additive favors to adjust the molecular packing toward face-on orientation and higher L_c along the OOP direction compared with the only one additive, which should be beneficial to realizing higher charge carrier mobility and FF in the OSC.

To clarify the interaction of OFP additive with PM6 donor and Y6 acceptor, we compared their miscibility by evaluating the surface energy (γ) *via* measuring the contact angles on water and diiodomethane (DIM) [44]. As shown in Figure S11 and Table S6, the γ was measured to be 34.08 mN m^{-1} for PM6, 39.77 mN m^{-1} for Y6, and 42.03 mN m^{-1} for OFP. Then, the blends miscibility was estimated by the Flory–Huggins interaction parameter (χ) [45]. The χ parameter of the Y6:OFP blend (χ=0.030) is lower than that of the PM6:OFP blend (χ=0.411), implying that the OFP additive has higher miscibility with Y6 acceptor as compared with PM6 donors. Therefore, the OFP additive mainly affects the aggregation of Y6 rather than PM6 during the film formation process.

The atomic force microscopy (AFM) and transmission electron microscopy (TEM) measurements were carried out to investigate the morphologies of the PM6:Y6 blend films processed with various additives. As depicted in Figure 5a, the PM6:Y6 blend film without any additive showed relatively uneven surface with root-mean-square surface roughness (R_q) of 1.03 nm. The addition of OFP or CN additive smoothed the surface to some extent, resulting in a slightly lower R_q of 0.92 and 0.93 nm, respectively. The R_q of blend film was further reduced to 0.81 nm when treated by the dual additives of OFP and CN. TEM measurement results (Figure 5b) revealed that the PM6:Y6 blend without the additive showed large and uneven phase separation with clearly oversized domain sizes. Such morphology was effectively restricted to realize appropriate phase separation with fibrous structure by using 0.5% CN additive. The undesirable phase separation in the PM6:Y6 blend was also tuned to some extent upon using 25% OFP as additive. Importantly, the dual additives of 25% OFP and 0.5% CN significantly established more favorable phase separation in the blend film than that processed by CN additive alone, facilitating to highly efficient exciton dissociation and charge transport. Relative to the blend film processed by CN or OFP additive, the more ordered stacking and smaller phase size established in the PM6:Y6 film treated by dual additives of CN and OFP effectively decreased the recombination center and suppressed the trap-assisted recombination. Note that the thickness of the PM6:Y6 blend processed by the dual additives of OFP and CN slightly decreased from 104±5 to 101±4 nm after the TA at 90 °C for 10 min, implying that the film was compressed with the OFP removing from the blend. On the other hand, the TA temperature below the glass transition temperature (T_g) has been proven to change the conformation of polymers [46], and therefore the local changes in the PM6 (T_g=193 °C [47]) conformation can be permitted under the TA at 90 °C in this case. Thus, we propose that the OFP additive has pronounced effect on restricting the over self-assembly of Y6 during the film formation under the synergistic effect with the CN additive. Afterwards, the respective self-assembly of PM6 and Y6 is refined towards appropriate phase separation networks during the kinetic process of OFP removal under the TA.

3 Conclusions

In summary, we have developed a commercially available

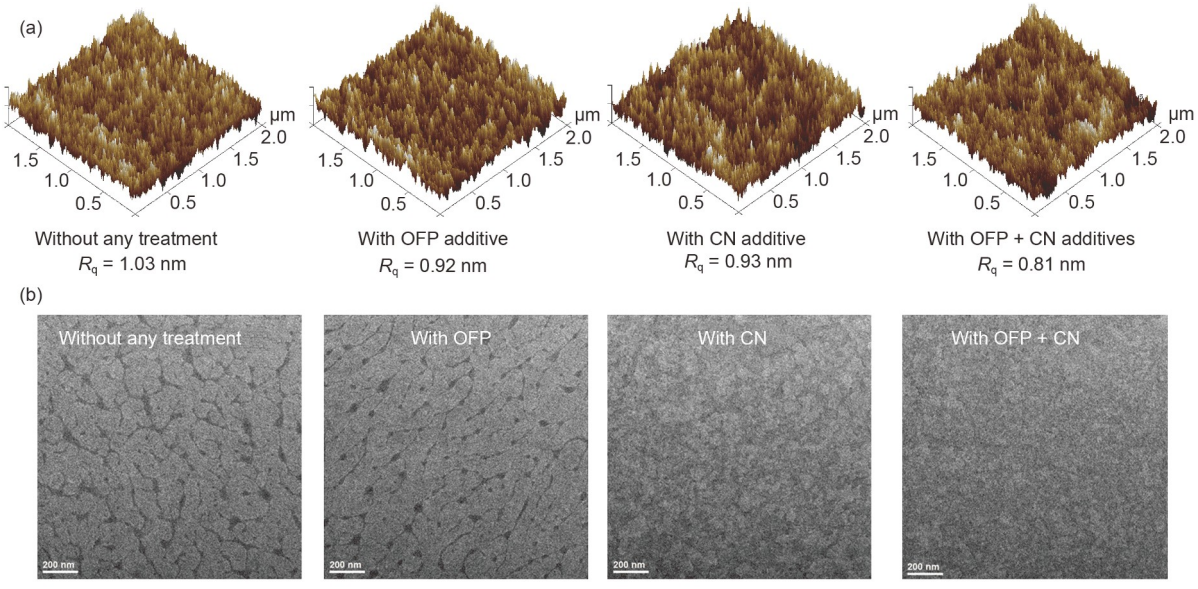

Figure 5 (a) AFM topography images and (b) TEM images of the PM6:Y6 (1:1.2, *w*/*w*) blend films processed with different additives (color online).

compound 4,4′-dimethoxyoctafluorobiphenyl (OFP) as a volatile solid additive to optimize BHJ morphology in OSCs. The strong crystallinity of OFP offers the possibility to restrict the over aggregation of non-fullerene acceptors with high crystallinity during the film cast process, leaving the well-established phase separation with nano-scale bi-continuous donor/acceptor interpenetrating networks after OFP volatilization by subsequent TA. Therefore, synergistic effect of CN and OFP dual additives showed supreme capability to further optimize the BHJ morphology over the conventional solvent additive, which is in favor of improving charge transport and suppressing charge recombination for higher FFs of the OSCs. As a result, relative to the CN additive alone, significantly improved FFs were obtained and led to higher PCEs in various OSC systems with the dual additives. In particular, the PTQ10:*m*-BTP–C6Ph-based device processed by the dual additives of CN and OFP showed a remarkable PCE of 17.74% associated with a notable FF of 0.783, while the control device processed by the CN additive alone yielded a lower PCE of 16.45% and a lower FF of 0.749. The results demonstrate the promising application of OFP as a solid additive in optimizing the BHJ morphology of OSCs toward better photovoltaic performances.

Acknowledgements This work is supported by the National Natural Science Foundation of China (22022509, 51873140 and 51820105003), Jiangsu Provincial Natural Science Foundation (BK20190095), Priority Academic Program Development of Jiangsu Higher Education Institutions (PAPD), and Collaborative Innovation Center of Suzhou Nano Science and Technology.

Conflict of interest The authors declare no conflict of interest.

Supporting information The supporting information is available online at http://chem.scichina.com and http://link.springer.com/journal/11426. The supporting materials are published as submitted, without typesetting or editing. The responsibility for scientific accuracy and content remains entirely with the authors.

1 Li Y, Xu G, Cui C, Li Y. *Adv Energy Mater*, 2018, 8: 1701791
2 Krebs FC, Espinosa N, Hösel M, Søndergaard RR, Jørgensen M. *Adv Mater*, 2014, 26: 29–39
3 Li G, Zhu R, Yang Y. *Nat Photon*, 2012, 6: 153–161
4 Servaites JD, Ratner MA, Marks TJ. *Energy Environ Sci*, 2011, 4: 4410
5 Facchetti A. *Mater Today*, 2013, 16: 123–132
6 Wei Q, Liu W, Leclerc M, Yuan J, Chen H, Zou Y. *Sci China Chem*, 2020, 63: 1352–1366
7 Cui C, Li Y. *Energy Environ Sci*, 2019, 12: 3225–3246
8 Li Y. *Acc Chem Res*, 2012, 45: 723–733
9 Yan C, Barlow S, Wang Z, Yan H, Jen AKY, Marder SR, Zhan X. *Nat Rev Mater*, 2018, 3: 18003
10 Lee C, Lee S, Kim GU, Lee W, Kim BJ. *Chem Rev*, 2019, 119: 8028–8086
11 Cai Y, Huo L, Sun Y. *Adv Mater*, 2017, 29: 1605437
12 Yao H, Wang J, Xu Y, Zhang S, Hou J. *Acc Chem Res*, 2020, 53: 822–832
13 Chen Y, Wan X, Long G. *Acc Chem Res*, 2013, 46: 2645–2655
14 Yu G, Gao J, Hummelen JC, Wudl F, Heeger AJ. *Science*, 1995, 270: 1789–1791
15 Heeger AJ. *Adv Mater*, 2013, 26: 10–28
16 Lin Y, Wang J, Zhang ZG, Bai H, Li Y, Zhu D, Zhan X. *Adv Mater*, 2015, 27: 1170–1174
17 Zhao W, Li S, Yao H, Zhang S, Zhang Y, Yang B, Hou J. *J Am Chem Soc*, 2017, 139: 7148–7151
18 Yuan J, Zhang Y, Zhou L, Zhang G, Yip HL, Lau TK, Lu X, Zhu C, Peng H, Johnson PA, Leclerc M, Cao Y, Ulanski J, Li Y, Zou Y. *Joule*, 2019, 3: 1140–1151
19 Wu Q, Wang W, Wang T, Sun R, Guo J, Wu Y, Jiao X, Brabec CJ, Li Y, Min J. *Sci China Chem*, 2020, 63: 1449–1460
20 Fan B, Zhang D, Li M, Zhong W, Zeng Z, Ying L, Huang F, Cao Y. *Sci China Chem*, 2019, 62: 746–752
21 Ma R, Liu T, Luo Z, Guo Q, Xiao Y, Chen Y, Li X, Luo S, Lu X, Zhang M, Li Y, Yan H. *Sci China Chem*, 2020, 63: 325–330
22 Cui C, Li Y. *Aggregate*, 2021, 2: e31
23 Zhao F, Wang C, Zhan X. *Adv Energy Mater*, 2018, 8: 1703147
24 Liao HC, Ho CC, Chang CY, Jao MH, Darling SB, Su WF. *Mater Today*, 2013, 16: 326–336
25 McDowell C, Abdelsamie M, Toney MF, Bazan GC. *Adv Mater*, 2018, 30: 1707114
26 Lee JK, Ma WL, Brabec CJ, Yuen J, Moon JS, Kim JY, Lee K, Bazan GC, Heeger AJ. *J Am Chem Soc*, 2008, 130: 3619–3623
27 Brady MA, Su GM, Chabinyc ML. *Soft Matter*, 2011, 7: 11065–11077
28 Peet J, Kim JY, Coates NE, Ma WL, Moses D, Heeger AJ, Bazan GC. *Nat Mater*, 2007, 6: 497–500
29 Yao Y, Hou J, Xu Z, Li G, Yang Y. *Adv Funct Mater*, 2008, 18: 1783–1789
30 Brinkmann M, Wittmann JC. *Adv Mater*, 2006, 18: 860–863
31 Müller C, Aghamohammadi M, Himmelberger S, Sonar P, Garriga M, Salleo A, Campoy-Quiles M. *Adv Funct Mater*, 2013, 23: 2368–2377
32 Kim JY, Yang DS, Shin J, Bilby D, Chung K, Um HA, Chun J, Pyo S, Cho MJ, Kim J, Choi DH. *ACS Appl Mater Interfaces*, 2015, 7: 13431–13439
33 Dörling B, Vohra V, Dao TT, Garriga M, Murata H, Campoy-Quiles M. *J Mater Chem C*, 2014, 2: 3303–3310
34 Vohra V, Dörling B, Higashimine K, Murata H. *Appl Phys Express*, 2015, 9: 012301
35 Fahey DP, Dougherty William G. J, Kassel WS, Wang X, Beckmann PA. *J Phys Chem A*, 2012, 116: 11946–11956
36 Beckmann PA, Mallory CW, Mallory FB, Rheingold AL, Wang X. *ChemPhysChem*, 2015, 16: 1509–1519
37 Chai G, Chang Y, Zhang J, Xu X, Yu L, Zou X, Li X, Chen Y, Luo S, Liu B, Bai F, Luo Z, Yu H, Liang J, Liu T, Wong KS, Zhou H, Peng Q, Yan H. *Energy Environ Sci*, 2021, 14: 3469–3479
38 Vandewal K, Widmer J, Heumueller T, Brabec CJ, McGehee MD, Leo K, Riede M, Salleo A. *Adv Mater*, 2014, 26: 3839–3843
39 Credgington D, Durrant JR. *J Phys Chem Lett*, 2012, 3: 1465–1478
40 Wu Y, Zheng Y, Yang H, Sun C, Dong Y, Cui C, Yan H, Li Y. *Sci China Chem*, 2020, 63: 265–271
41 Mihailetchi VD, Koster LJA, Hummelen JC, Blom PWM. *Phys Rev Lett*, 2004, 93: 216601
42 Schilinsky P, Waldauf C, Brabec CJ. *Appl Phys Lett*, 2002, 81: 3885–3887
43 Koster LJA, Mihailetchi VD, Ramaker R, Blom PWM. *Appl Phys Lett*, 2005, 86: 123509
44 Owens DK, Wendt RC. *J Appl Polym Sci*, 1969, 13: 1741–1747
45 Nilsson S, Bernasik A, Budkowski A, Moons E. *Macromolecules*, 2007, 40: 8291–8301
46 Bergqvist J, Lindqvist C, Bäcke O, Ma Z, Tang Z, Tress W, Gustafsson S, Wang E, Olsson E, Andersson MR, Inganäs O, Müller C. *J Mater Chem A*, 2014, 2: 6146–6152
47 Han J, Bao F, Huang D, Wang X, Yang C, Yang R, Jian X, Wang J, Bao X, Chu J. *Adv Funct Mater*, 2020, 30: 2003654